

## CHAPTER 4

### Towards a Second-Generation Receptor Site for Bacterial Spore Detection

## 4.1 Introduction

To improve upon our first-generation receptor site, we have two general directions to pursue: (1) alter the architecture of the macrocyclic ligand to improve binding affinity for dipicolinate, at the risk of losing some of the advantages of the current ligand, or (2) modify the ligand slightly to append the complex to a solid substrate and improve the limit of detection for dipicolinate as opposed to the binding affinity. The first method, though seemingly straightforward, can be quite difficult to implement. We could predict through structural simulations, for example, that attaching phenyl moieties on the carboxyl arms of the DO2A ligand might enhance dipicolinate binding affinity through stabilization due to pi-stacking. However, such modifications to the DO2A ligand would most likely severely limit solubility of the complex and have a variety of other unexpected effects on properties. We therefore aim to retain the demonstrated advantages of the DO2A ligand and improve upon bacterial spore detection through attaching the dipicolinate sensing complex to a solid matrix. This strategy could resolve multiple issues regarding bacterial spore imaging and current limits of detection in environmental samples.

Appending the  $\text{Tb}(\text{DO2A})^+$  complex to polydimethylsiloxane (PDMS) could significantly improve our microscopic endospore viability assay ( $\mu\text{EVA}$ ) developed to image bacterial spores. In this assay, endospores are inoculated onto wells of agarose doped with  $\text{TbCl}_3$  and induced to germinate via the addition of either L- or D-alanine for aerobic or anaerobic spores, respectively. As the bacterial spores germinate and return to the normal vegetative cycle, their DPA is released and binds to the  $\text{Tb}^{3+}$  ions in the agarose. The resulting ‘halos’ of  $\text{Tb}(\text{DPA})_n$  complexes ( $n = 1-3$ ) around each endospore

are visible using time-gated fluorescence microscopy.<sup>1-3</sup> In the current protocol, certain species of endospore are more easily observed than others. This is due to the fact that  $\mu$ EVA only images bacterial spores that are capable of germination, and the rate of germination varies significantly between spore species. Germination occurs when endospores are triggered to reenter the normal vegetative cell cycle, during which they release DPA into the environment. *Bacillus* spores germinate relatively quickly, on the order of minutes. *Clostridium* spores, however, exhibit germination profiles on the order of hours to even days.<sup>4</sup> For these slow germinating species, the rate of DPA diffusion begins to outcompete the rate of germination, and little or no signal results in  $\mu$ EVA. PDMS is used as a 'coverslip' in  $\mu$ EVA to slow drying of the agarose, limit DPA diffusion and improve image quality. However, we have yet to explore its potential to serve as a synthon upon which DPA binding receptor sites can be covalently bound. By appending the Tb-macrocycle complex to the PDMS, we may be able to significantly lengthen the residence time of DPA proximal to the endospore that released it, elongating our imaging window. Additionally, another problem encountered with  $\mu$ EVA involves the microscopy. The agarose surface on which the spores sit is often uneven due to multiple variables in its preparation, meaning that not all spores are present on the same focal plane, rendering an accurate enumeration in any single microscopic view impossible. But, if the DPA released from the germinating spores is effectively bound to a Tb-macrocycle complex that is itself covalently attached to the PDMS coverslip, the PDMS is the only surface necessary to image. The PDMS could be peeled off of the agarose following germination, placed on a flat surface and imaged separately, eliminating the problem of multiple focal planes.

Another mode of improvement via construction of a solid-state bacterial spore sensor lies in sample concentration to enhance the current limit of detection. If the terbium-macrocycle complex were covalently bound to the stationary phase of a column, such as silica or alumina, a dilute DPA solution could be readily concentrated. When applied to environmental samples this protocol would involve sample collection, DPA release via physical (heating, pressure) or chemical (germinant or lysozyme) means, and filtration to remove any cell debris or other material. The dilute DPA solution, buffered to pH 7–10, could then be passed through the column containing  $\text{Tb}(\text{DO2A})^+$  bound to the solid substrate. The high binding affinity of the terbium-macrocycle binary complex for DPA at this pH would cause the dipicolinate to be retained in the column. After saturation, the addition of a small aliquot of acidic solution (pH  $\sim$  2) will protonate the macrocyclic ligand and release the  $\text{Tb}(\text{DPA})^+$  complex, which could then be quantified using fluorescence spectroscopy and correlated to the original filtrate volume to yield a value of spores per mL of solution. The column could then be treated with a  $\text{TbCl}_3$  solution at neutral pH to reform the terbium-macrocycle complex in the solid phase for reuse. Current limits of detection of bacterial spores in environmental samples for spectroscopic techniques are in the  $10^3$ – $10^4$  spores/mL range.<sup>5-7</sup> This technology could improve the current limit of detection of bacterial spores by several orders of magnitude.

We therefore explore a novel macrocyclic ligand DOAAM (*1,4,7,10-tetraazacyclododecane-1-acetate-7-amide*) bound to terbium as the next step in achieving this goal. We have chosen to replace one of the acetate pendant arms with an amide functional group, because the primary amide can be easily functionalized to append the ligand to a solid substrate without perturbing the hexadentate chelation motif to the

lanthanide (Figure 4.1). The neutral tetraamide derivative DOTAM (*1,4,7,10-tetraazacyclododecane-1,4,7,10-tetraamide*) is known to strongly bind lanthanides in the same configuration as DOTA, with coordination through the four ring nitrogen atoms and four amide oxygen atoms.<sup>8,9</sup> However, binding affinity is approximately 10–15 orders of magnitude less than the DOTA ligand (Table 4.1),<sup>10-13</sup> presumably due to the lower basicity of the ring N-atoms and the loss of electrostatic attraction for the neutral amide ligands compared to the acetate groups. The absence of protonated intermediates in the complexation of lanthanides also distinguishes the DOTAM ligand from DOTA.<sup>14</sup> However, with modification of only one pendant arm, any loss in lanthanide chelation should be minimal and electrostatics should dominate the observed binding interactions.

We will fully characterize our second-generation Tb(DOAAM)<sup>2+</sup> dipicolinate receptor site in terms of photophysics, binding affinity and pH dependence. We will also discuss future techniques to anchor this complex in the process of constructing a solid-state sensor.

## 4.2 Photophysics and Structure

With the substitution of an amide for one of the DO2A acetate groups, the DOAAM ligand should still coordinate the lanthanide in a hexadentate fashion. Due to the oxophilic character of lanthanide binding and reported work with the DOTAM ligand, we anticipate binding via the oxygen of the amide with negligible change in symmetry of the lanthanide coordination sphere. The replacement of an OH with an NH-oscillator may increase the quantum yield of the Tb(DOAAM)(DPA) complex compared to its DO2A analogue.

#### 4.2.1 Structural Characterization

We will attempt to crystallize the Tb(DOAAM)(DPA) ternary complex for complete characterization. If high quality crystals cannot be obtained, the complex will be characterized using elemental analysis and mass spectrometry.

#### Experimental Section

**Materials.** The following chemicals were purchased and used as received: acetone (J. T. Baker), acetonitrile (Fluka Biochemika), ammonium hydroxide (28.0–30.0% in water) (J. T. Baker), DPA (dipicolinic acid, pyridine-2,6-dicarboxylic acid) (Aldrich), ethyl alcohol (200-proof) (Acros Organics), hydrochloric acid (36.5–38.0% in water) (EMD Chemicals), isopropyl alcohol (2-propanol) (J. T. Baker), methanol (J. T. Baker), potassium carbonate anhydrous (Alfa Aesar), sodium carbonate anhydrous (Mallinckrodt), sodium hydroxide (NaOH 50% in water) (Mallinckrodt), terbium (III) chloride hexahydrate (Alfa Aesar) and tetrahydrofuran (THF) (EM Science). All lanthanide salts were 99.9% pure or greater, all solvents were ACS certified or HPLC grade, and all other salts were 99% pure or greater. The DOAAM ligand (*1,4,7,10-tetraazacyclododecane-1-acetate-7-amide*) was synthesized under contract by Macrocyclics (Ref. GKRD02-38-080121). See Appendix G for characterization. Water was deionized to a resistivity of 18.2 M $\Omega$ -cm using a Purelab® Ultra laboratory water purification system (Siemens Water Technologies, Warrendale, PA).

**Methods.** Crystallization attempts included use of various solvent systems (water, methanol, ethanol, isopropanol and THF), with different bases for pH adjustment (NaOH, NH<sub>4</sub>OH). Extraction with hot solvent (water or isopropanol), freezing saturated

solvents, and various double-boiler combinations (acetone/ethanol, acetone/isopropanol) were also attempted. In the double-boiler method, a saturated solution containing the complex was placed in an open vial in a sealed container with another miscible solvent of high vapor pressure in which the complex is less soluble (acetone in this case). Slow diffusion of this solvent into the saturated solution should reduce the solubility of the complex and induce crystallization. However, this only led to precipitation for the Tb(DOAAM)(DPA) complex.

We also attempted phase separation with isopropanol and a saturated aqueous solution of  $\text{Na}_2\text{CO}_3$ , which causes the normally miscible solvents to separate and produced a solution of Tb(DOAAM)(DPA) in the isopropanol layer. This solution, when placed in a double-boiler with acetone, formed small filamentous crystals after three days that were luminescent under UV illumination. However, these were not of crystallographic quality and the method did not produce sufficient sample for characterization using elemental analysis or mass spectrometry. This was repeated with  $\text{K}_2\text{CO}_3$  instead of  $\text{Na}_2\text{CO}_3$ , but only produced precipitation.

In a clean, kilned 30-mL beaker, 0.30791 g (0.830 mmol) of  $\text{TbCl}_3 \cdot 6\text{H}_2\text{O}$  and 0.24218 g (0.843 mmol) of DOAAM were combined in 2.0 mL of nanopure water (18.2  $\text{M}\Omega\text{-cm}$  resistivity) and sonicated to dissolve. The clear yellow solution was already near neutral (pH 6.5), so 0.13130 g (0.786 mmol) of DPA was added, along with 4.0 mL of nanopure water. The pH of the opaque white solution was adjusted to  $\sim 7$  with a saturated  $\text{Na}_2\text{CO}_3$  solution, added dropwise, while stirring with gentle heating (40  $^\circ\text{C}$ ). Solution clarification was not observed. Following positive identification of the ternary complex via fluorescence spectroscopy (equilibration time of 2 days), the solution was lyophilized

using a MicroModulyo Freeze Dryer (Thermo Electron Corporation, Waltham, MA) to dryness (2 days). The solid was redissolved in ~ 7 mL of pure (200-proof) ethanol and filtered using a fine frit (Pyrex, 15mL, ASTM 4-5.5F) into a new scintillation vial (rinsed 2 times with ethanol and 2 times with filtered ethanol to remove any particulates). This vial, with cap cracked open slightly, was placed in a double-boiler with acetone in the outer container. Precipitation of a white solid from the clear, colorless solution was observed after 1.5 hours. The ethanol was decanted and the solid lyophilized to dryness. The resulting white powdery precipitate was characterized using elemental analysis and mass spectrometry.

Elemental analysis and mass spectrometry were performed by Desert Analytics Transwest Geochem and the Caltech mass spectrometer facility, respectively, as previously described (Section 2.2.1).

### Results and Discussion

Despite many attempts to crystallize the ternary complex using a plethora of solvent systems and techniques, no high quality crystals could be obtained, possibly due to the lack of a counterion for the neutral Tb(DOAAM)(DPA) complex. Regardless, the pure compound was obtained as a precipitate (0.15661 g, yield: 21.3%), and positively identified via elemental analysis and mass spectrometry. Anal. Calcd (found) in duplicate for  $\text{TbC}_{19}\text{H}_{27}\text{N}_6\text{O}_7 \cdot 2.8\text{NH}_4 \cdot 1.0\text{CO}_3 \cdot 3.2\text{C}_2\text{H}_6\text{O} \cdot 1.6\text{Cl} \cdot 0.5\text{OH}$  (fw = 934.65): C, 33.90 (33.90); H, 6.27 (5.07); N, 13.25 (13.30); Tb, 17.00 (16.97); Cl, 6.20 (6.20). ESI-MS ( $m/z$ ): calcd (found) for  $\text{TbC}_{19}\text{H}_{28}\text{N}_6\text{O}_7$  (M + H) 611.4 (611.1).

#### 4.2.2 Spectroscopy

We will explore the absorbance, excitation and emission spectra of the Tb(DOAAM)(DPA) complex to determine if the structural modification has altered binding geometry or spectroscopic response. If the DOAAM ligand is coordinating to the lanthanide in a different fashion than the DO2A ligand, such as via the amide nitrogen as opposed to the oxygen, this will significantly alter the symmetry of the lanthanide coordination sphere and should therefore result in unique fine structure in the emission spectrum (Section 2.3.1). Similarly, any changes in the chelation mode or distance of the dipicolinate ligand should be evident in a shift of the excitation spectrum, as previously seen for the F-DPA and Pic ligands (Section 3.3).

#### Experimental Section

**Materials.** MOPS (3-(*N*-morpholino)ethanesulfonic acid) buffer (Alfa Aesar) was purchased and used as received. Dried, fully characterized TBA·Tb(DO2A)(DPA) crystals (Section 2.2.1) or Tb(DOAAM)(DPA) precipitate were used to generate a 1:1:1 ratio of Tb/macrocycle/dipicolinate in solution. Water was deionized to a resistivity of 18.2 MΩ-cm using a Purelab® Ultra laboratory water purification system.

**Methods.** Solutions of 10.0 μM Tb(DO2A)(DPA)<sup>-</sup> and Tb(DOAAM)(DPA) were prepared in 0.1 M MOPS buffer (pH 7.3) in triplicate in disposable acrylate cuvettes (Specrocell, Oreland, PA) with a 1 cm path length and allowed to equilibrate for 24 hours. Luminescence spectral analysis was performed by a Fluorolog Fluorescence Spectrometer (Horiba Jobin-Yvon, Edison, NJ) at 25 °C. To prevent second-order diffraction of the source radiation, all measurements were taken with a 350-nm colorless

sharp cutoff glass filter (03 FCG 055, Melles Griot, Covina, CA). The solution pH was measured using a calibrated handheld pH/mV/temperature meter (Model IQ150, I. Q. Scientific Instruments, Loveland, CO) following data collection. All reported spectra were obtained as a ratio of corrected signal to corrected reference ( $S_c/R_c$ ) to eliminate the effect of varying background radiation in the sample chamber; intensities are in units of counts per second per microampere (cps/ $\mu$ A).

### Results and Discussion

The normalized excitation and emission spectra of the Tb(DOAAM)(DPA) complex are identical to that of the Tb(DO2A)(DPA)<sup>-</sup> complex (Figures 4.2 and 4.3), indicating that the symmetry and composition of the lanthanide coordination sphere is unaffected by the acetate/amide substitution. This strongly suggests that the amide moiety is coordinating via the oxygen as opposed to the nitrogen, and that the arrangement around the terbium cation remains in a slightly distorted capped staggered square bipyramidal conformation (Section 2.2.2). The intensity of the emission spectrum for the Tb(DOAAM)(DPA) complex is also nearly twofold greater than that of the Tb(DO2A)(DPA)<sup>-</sup> complex; this will be addressed in the next section (vide infra).

#### 4.2.3 Quantum Yield

As described in Section 2.3.2, we define luminescence quantum yield ( $\Phi_L$ ) as the ratio of photons absorbed by the chromophore to photons emitted through luminescence from the lanthanide following energy transfer. We will measure the luminescence quantum yield of Tb(DOAAM)(DPA) with respect to the L-tryptophan standard used

previously, and compare this value to that of the DO2A complex. As mentioned in Chapter 1, OH oscillators are the greatest quenchers of lanthanide luminescence; replacement of an OH oscillator with an NH group should therefore reduce quenching and result in enhanced quantum yield for the DOAAM complex.

### Experimental Section

**Materials.** Tris buffer (tris-[hydroxymethyl]aminomethane) (MP Biomedicals, LLC) and L-tryptophan (Alfa Aesar) were purchased and used as received. Dried, fully characterized Tb(DOAAM)(DPA) precipitate was used to generate a 1:1:1 ratio of Tb/macrocycle/dipicolinate in solution. Water was deionized to a resistivity of 18.2 M $\Omega$ -cm using a Purelab® Ultra laboratory water purification system.

**Methods.** Five concentrations ranging from 5.0 to 15.0  $\mu$ M were prepared for the Tb(DOAAM)(DPA) complex in 0.1 M Tris buffer (pH 7.9) and the L-Trp standard in nanopure water (pH 4.5). Absorbance and luminescence measurements were made in quartz cuvettes (1 cm path length) using a Cary 50 Bio UV/Visible Spectrophotometer (Varian, Inc., Palo Alto, CA), and a Fluorolog-3 Fluorescence Spectrometer ( $\lambda_{\text{ex}} = 280$  nm). Absorbance measurements were zeroed to an empty quartz cuvette in the sample chamber; quartz cuvettes containing solvent only were run in triplicate as a control, so no baseline correction was performed. All recorded absorbances were under 0.1 and all luminescence intensities were below  $5 \times 10^5$  cps, well within the linear range of both instruments. Quartz cuvettes were cleaned using a nitric acid (50% in nanopure water) digest and rinsed thoroughly with nanopure water between samples. No background fluorescence was observed for the solvents used. The quantum yield was calculated

using equation 2.1 as described previously (Section 2.3.2) with L-tryptophan in nanopure water as the standard ( $\Phi_{\text{ref}} = 0.13 \pm 0.01$ ).<sup>15</sup> The molar extinction coefficient was calculated by plotting absorbance against concentration (Figure 4.4).

### Results and Discussion

The molar extinction coefficient for the Tb(DOAAM)(DPA) complex is  $2902 \pm 94 \text{ M}^{-1}\text{cm}^{-1}$ , in the same range of the Tb(DO2A)(DPA)<sup>-</sup> complex ( $2259 \pm 10 \text{ M}^{-1}\text{cm}^{-1}$ ) and the dipicolinate ligand ( $2832 \pm 21 \text{ M}^{-1}\text{cm}^{-1}$ ) as would be expected. The calculated molar extinction coefficient of the tryptophan standard ( $\epsilon_{\text{Exp}} = 5494 \text{ M}^{-1}\text{cm}^{-1}$ ) was within 1% of the reported value ( $\epsilon_{\text{Exp}} = 5502 \text{ M}^{-1}\text{cm}^{-1}$ ).

The luminescent quantum yield of the Tb(DOAAM)(DPA) complex is nearly twice as large as that of the Tb(DO2A)(DPA)<sup>-</sup> complex (Table 4.2). As these complexes have the same chromophore and lanthanide, and therefore the energy gap between the chromophore triplet and the lanthanide excited state is unchanged, we attribute this increase to a reduction in quenching. According to the superimposable emission spectra, the terbium coordination sphere is identical in terms of symmetry and composition; the quenching must therefore be an outer-sphere effect, most likely due to the acetate/amide substitution. Even though the change from OH to NH in this substitution is not in the inner-coordination sphere, the reduction in quenching is still substantial, confirming the strong influence of outer-sphere effects on lanthanide photophysics.<sup>16, 17</sup>

### 4.3 Binding Studies

The replacement of a negatively charged acetate by a neutral amide in the DOAAM ligand increases the overall charge of the binary complex from  $\text{Tb}(\text{DO2A})^+$  to  $\text{Tb}(\text{DOAAM})^{2+}$  at neutral pH. Due to the increase in electropositive charge for the receptor site, we might anticipate a greater electrostatic attraction for the  $\text{DPA}^{2-}$  analyte and therefore an increase in dipicolinate binding affinity. However, previous investigations have shown that ‘ligand enhancement’ of lanthanide-analyte binding affinity can often be independent of the net electrostatics of the system, and may depend more on changes in the local environment of the binding site in the lanthanide coordination sphere (Section 3.7). Spectroscopic studies suggest that the DOAAM ligand chelates to the lanthanide in the same fashion as DO2A, with presumably the same ‘footprint’ and leaving a binding cavity of similar size and shape. If these assumptions are valid, the local electrostatics in the binding site should be similar in both cases, and if this is indeed the dominant factor in dipicolinate coordination, the binding affinity may not change significantly.

#### 4.3.1 Jobs Plots

A method of continuous variations was applied to determine the binding stoichiometry of dipicolinate to the  $\text{Tb}(\text{DOAAM})^{2+}$  binary complex. The replacement of an acetate arm by an amide may destabilize the  $\text{Tb}(\text{DOAAM})^{2+}$  binary complex, but as the ligand is hexadentate we still anticipate a 1:1 binding ratio of binary complex to dipicolinate.

## Experimental Section

**Materials.** The following chemicals were purchased and used as received: DPA (dipicolinic acid, pyridine-2,6,-dicarboxylic acid) (Aldrich), sodium acetate trihydrate (Mallinckrodt) and terbium(III) chloride hexahydrate (Alfa Aesar). All lanthanide salts were 99.9% pure or greater and all other salts were 98% pure or greater. The DOAAM ligand was synthesized by Macrocyclics (Section 4.2.1). Water was deionized to a resistivity of 18.2 M $\Omega$ -cm using a Purelab® Ultra laboratory water purification system.

**Methods.** All samples were prepared in triplicate from stock solutions to a final volume of 3.50 mL in disposable acrylate cuvettes (Spectrocell, Oreland, PA) with a 1 cm path length and were allowed to equilibrate for at least 6 days prior to analysis. The concentrations of TbCl<sub>3</sub> and DPA were varied inversely in 1.0- $\mu$ M increments from 0 to 12.0  $\mu$ M with 100  $\mu$ M DOAAM in 0.2 M NaOAc, pH 7.4.

Luminescence spectral analysis was performed by a Fluorolog Fluorescence Spectrometer with a 350-nm cutoff filter as previously described (Section 4.2.2). The solution pH was measured using a calibrated handheld IQ150 pH/mV/temperature meter (I. Q. Scientific Instruments) following data collection.

## Results and Discussion

According to the Jobs plot (Figure 4.5), the optimal binding stoichiometry for DPA to Tb(DOAAM)<sup>2+</sup> occurs at a terbium mole fraction of approximately 0.5, meaning a one-to-one correlation. However, the flattened appearance of the plot indicates low to moderate stability of the complex,<sup>18</sup> especially at high DPA concentrations. This is consistent with reports of lower stability constants for amide-substituted macrocyclic

ligands compared to their acetate analogs.<sup>10, 11</sup> Though the stability of the complex appears to have diminished, we still see linearity in the range of high terbium mole fraction, meaning the Tb(DOAAM)<sup>2+</sup> complex can bind dipicolinate effectively when in excess.

#### 4.3.2 Calculation of Dipicolinate Association Constant

Though the Tb(DOAAM)(DPA) complex could not be successfully crystallized, we were able to fully characterize a solid precipitate of this complex. As this solid is consistent in terms of its Tb/DOAAM/DPA ratio, we can still perform the binding affinity by competition (BAC) assay to determine the DPA to binary complex binding constant.

### Experimental Section

**Materials.** Terbium(III) chloride hexahydrate (Alfa Aesar) was purchased and used as received. All lanthanide salts were 99.9% pure or greater and all other salts were 97% pure or greater. Dried, fully characterized Tb(DOAAM)(DPA) precipitate was used to produce a 1:1:1 ratio of Ln:DO2A:DPA in solution. Water was deionized to a resistivity of 18.2 M $\Omega$ -cm using a Purelab® Ultra laboratory water purification system.

**Methods.** All samples were prepared to a final volume of 3.50 mL from stock solutions in disposable acrylate cuvettes (Spectrocell) with a 1 cm path length and were allowed to equilibrate for 5 days. Luminescence spectral analysis was performed by a Fluorolog Fluorescence Spectrometer with a 350-nm cutoff filter as previously described (Section 4.2.2). The solution pH was measured using a calibrated handheld IQ150

pH/mV/temperature meter (I. Q. Scientific Instruments) following data collection. Sample temperature was monitored using a handheld Fluke 62 Mini Infrared Thermometer (Fluke Corp, Everett, WA).

Samples were prepared using solvated Tb(DOAAM)(DPA) precipitate and terbium chloride in 0.2 M sodium acetate (pH 7.4), such that the concentration of Tb(DOAAM)(DPA) was 1.0  $\mu\text{M}$  and the concentration of free  $\text{Tb}^{3+}$  ranged from 1.0 nM to 1.0 mM. As  $\text{Tb}^{3+}$  was added, the shift in equilibrium Tb(DOAAM)(DPA) and  $\text{Tb(DPA)}^+$  concentrations was monitored via a ligand field sensitive transition in the emission spectrum using luminescence spectroscopy. Emission spectra ( $\lambda_{\text{ex}} = 278 \text{ nm}$ ) were integrated over the most ligand-field sensitive peak ( ${}^5\text{D}_4 \rightarrow {}^7\text{F}_4$ , 570–600 nm) to produce a curve of observed integrated intensity ( $I_{\text{obs}}$ ) against the log of excess free lanthanide ( $\log [\text{Ln}^{3+}]_{\text{xs}}$ ). A best fit to a two-state thermodynamic model using the Curve Fitting Tool in Matlab® yielded the competition equilibrium constant ( $K_{\text{c}}$ ) and dipicolinate affinity constant ( $K_{\text{a}}'$ ) as described previously (Section 3.2.2).

## Results and Discussion

Despite the fact that no crystals could be obtained for the Tb(DOAAM)(DPA) complex, the competition assay using the characterized precipitate still produced a curve that could be fit using the two-state thermodynamic model (Figure 4.6). The use of the precipitate as opposed to crystals for the Tb(DOAAM)(DPA) complex demonstrates the power and versatility of the BAC assay. As long as a 1:1:1 ratio of the three components can be obtained, whether via high quality crystals or a fully characterized precipitate, the method can be applied and will produce a binding constant with acceptable error.

The binding affinity for dipicolinate decreases slightly from the  $\text{Tb}(\text{DO2A})^+$  complex to the  $\text{Tb}(\text{DOAAM})^{2+}$  complex (Table 4.3), despite the increase in electrostatic attraction between the complex and the  $\text{DPA}^{2-}$  dianion. This is most likely due to (1) the replacement of the acetate arm with an amide group, which is not as electronegative and not as capable of perturbing the electron density of the  $\text{Tb}^{3+}$  ion, and (2) decreased stability of the complex, as evidenced by the nonlinear Jobs plot and previous studies with similar amide-substituted macrocyclic ligands. The negligible change in dipicolinate binding affinity despite an increase in binary complex charge is consistent with our hypothesis that net electrostatics do not dominate in these systems involving ‘ligand enhancement’. Instead, the ability of the ligand to shift the electron density of the lanthanide cation, thereby generating a binding cavity with more local electropositive charge, might be a better explanation. We see an improvement in dipicolinate binding affinity over the  $\text{Tb}^{3+}$  ion alone, but the less-electronegative amide group of the DOAAM ligand is not as effective at perturbing the electron density of the lanthanide as the dual-acetate arms of the DO2A ligand. Hence, binding studies with the DOAAM ligand support the theory of ‘ligand enhancement’ due to ligand-induced perturbation of lanthanide electron density, and confirm that the correct choice of helper ligand is significant in order to maximize analyte binding affinity.

#### 4.4 pH Dependence

The stability of the  $\text{Tb}(\text{DOAAM})(\text{DPA})$  complex in terms of pH variations will be determined and compared to the  $\text{Tb}(\text{DO2A})(\text{DPA})^-$  complex. The acetate/amide substitution of the macrocyclic ligand will invariably shift the  $\text{pK}_a$  of that chelating arm

substantially. However, as primary amides tend to resist deprotonation and only form weak conjugate acids, this substituent will most likely remain neutral over the pH range of interest and therefore the relative stability of the complex should remain constant.

### Experimental Section

**Materials.** The following chemicals were purchased and used as received: CAPS (1-cyclohexyl-3-aminopropanesulfonic acid) buffer (Alfa Aesar), CHES (*N*-cyclohexyl-2-aminoethanesulfonic acid) buffer (Alfa Aesar), MES monohydrate (2-(*N*-morpholino)ethanesulfonic acid monohydrate) buffer (Alfa Aesar), MOPS (3-(*N*-morpholino)-propanesulfonic acid) buffer (Alfa Aesar), sodium hydroxide (NaOH 50% in water) (Mallinckrodt) and TAPS (*N*-tris(hydroxymethyl)methyl-3-aminopropanesulfonic acid) buffer (TCI America). All salts were 99% pure or greater, and all buffers were at least 98% pure. Dried, fully characterized TBA·Tb(DO2A)(DPA) crystals (Section 2.2.1) or Tb(DOAAM)(DPA) precipitate were used to generate a 1:1:1 ratio of Tb/macrocycle/dipicolinate in solution. Water was deionized to a resistivity of 18.2 MΩ·cm using a Purelab® Ultra laboratory water purification system.

**Methods.** Samples of 10.0 μM pre-equilibrated Tb(DO2A)(DPA)<sup>-</sup> or Tb(DOAAM)(DPA) were prepared in 0.1 M buffer. Five buffers were used: MES (pK<sub>a</sub> = 6.1), MOPS (pK<sub>a</sub> = 7.2), TAPS (pK<sub>a</sub> = 8.4), CHES (pK<sub>a</sub> = 9.3) and CAPS (pK<sub>a</sub> = 10.4), with pH adjustment to within 0.1 of the pK<sub>a</sub> value using 50% NaOH added dropwise. Emission spectra were obtained after an equilibration time of 21 hours.

## Results and Discussion

The pH dependence study suggests that the DOAAM ligand behaves in a similar manner to the DO2A ligand in terms of retaining the lanthanide in solution and preventing precipitation of the hydroxide species in alkaline conditions. This is interesting, as previous studies indicate a severe loss in lanthanide chelation when the acetate arms of the macrocycle are substituted for amide moieties. Apparently the stability of the complex is still great enough to resist changes in pH over a range from 6.1 to 10.4, meaning the correlation between luminescence intensity and dipicolinate concentration is maintained.

### **4.5 Conclusions**

Binding studies of the  $\text{Tb}(\text{DOAAM})^{2+}$  and  $\text{Tb}(\text{DO2A})^+$  complexes indicate that substitution of an amide group for an acetate arm in the macrocyclic ligand destabilizes the binary complex and reduces affinity slightly for dipicolinate, despite the increase in electropositive charge of the complex. However, this decrease in stability is not evident in the pH dependence of the  $\text{Tb}(\text{DOAAM})(\text{DPA})$  complex, most likely due to the ternary complex maintaining a constant neutral state over the pH range studied.

The minor change in dipicolinate binding constant despite a difference in charge for the two terbium(macrocycle) complexes studied supports the interesting theory that net electrostatic attractions do not dominate in systems involving 'ligand enhancement'. Instead, the localized electrostatic charge of the binding site, generated by the ability of the helper ligand to perturb the electron density of the lanthanide, may play the defining role. Electron withdrawing effects of the helper ligand generate an increased positive

charge at the dipicolinate binding site, the magnitude of which is governed by the polarizability of the lanthanide and the number and arrangement of O and N moieties on the ligand. By replacement of an acetate with a less electronegative amide group, we have decreased the ability of the ligand to perturb the electron density of the lanthanide, resulting in a decrease in analyte binding affinity. However, further work involving binding affinities of lanthanide(macrocycle) complexes for other aromatic anions (picolinate, isophthalate, 2,2'-bipyridine, etc.) using various macrocyclic ligands of different charge and denticity should be explored.

With the replacement of an acetate arm on the macrocyclic ligand with an amide, we have maintained a nanomolar detection sensitivity for dipicolinate while nearly doubling the luminescence quantum yield. Studies also indicate that amide-substituted macrocyclic ligands, when bound to lanthanides, produce kinetically inert complexes with respect to acid-catalyzed dissociation,<sup>13</sup> meaning this complex could function as a robust in situ sensor. Though the DOAAM ligand appears to produce a less stable complex than DO2A, the increased quantum yield coupled to functionality of tethering this complex to a solid substrate makes  $\text{Tb}(\text{DOAAM})^{2+}$  a suitable second-generation dipicolinate receptor and puts us one step closer to reaching the ideal receptor site for bacterial spore detection (Figure 4.8).

The next step in the enhancement of bacterial spore detection is to covalently attach the  $\text{Tb}(\text{DOAAM})^{2+}$  complex to a solid substrate. As previously discussed, if this substrate is flexible and UV light-permeable, such as PDMS, we could use the  $\text{Tb}(\text{DOAAM})$ -functionalized surface to improve the microscopic endospore viability assay. Appending the  $\text{Tb}(\text{DOAAM})^{2+}$  complex to silica or alumina could also improve

the limit of detection of bacterial spores through concentration of environmental samples. In both cases, attachment to the substrate surface would most likely involve click chemistry or similar techniques, such as a Michael addition of a thiol-functionalized macrocycle to a vinyl-sulfone derivatized surface.<sup>19-22</sup> Macrocyclic ligands such as DOTA and DO2A have been conjugated to various target vectors and supramolecular architectures such as lipids, dendrimers and amino acids via similar methods.<sup>23-26</sup> With the high stability and robust quality of these lanthanide-macrocycle binary complexes, we believe the resulting dipicolinate-binding surfaces will significantly improve bacterial spore detection technologies.

## REFERENCES

- (1) Yung, P. T.; Ponce, A. *Applied and Environmental Microbiology* **2008**, *74*, 7669-7674.
- (2) Yung, P. T.; Kempf, M. J.; Ponce, A. *IEEE Aerospace Conference* **2006**, 1-13.
- (3) Yang, W.-W.; Ponce, A. *International Journal of Food Microbiology* **2009**, *133*, 213-216.
- (4) Yang, W.-W., California Institute of Technology, Pasadena, 2009.
- (5) Hindle, A. A.; Hall, E. A. H. *Analyst* **1999**, *124*, 1599-1604.
- (6) Pellegrino, P. M.; Fell, N. F.; Rosen, D. L.; Gillespie, J. B. *Analytical Chemistry* **1998**, *70*, 1755-1760.
- (7) Cable, M. L.; Kirby, J. P.; Sorasaene, K.; Gray, H. B.; Ponce, A. *J. Am. Chem. Soc.* **2007**, *129*, 1474-1475.
- (8) Amin, S.; Morrow, J. R.; Lake, C. H.; Churchill, M. R. *Angewandte Chemie-International Edition* **1994**, *33*, 773-775.
- (9) Amin, S.; Voss, D. A.; Horrocks Jr., W. D.; Lake, C. H.; Churchill, M. R.; Morrow, J. R. *Inorganic Chemistry* **1995**, *34*, 3294-3300.
- (10) Voss, D. A.; Farquhar, E. R.; Horrocks Jr., W. D.; Morrow, J. R. *Inorganica Chimica Acta* **2004**, *357*, 859-863.
- (11) Baranyai, Z.; Brücher, E.; Iványi, T.; Király, R.; Lázár, I.; Zékány, L. *Helvetica Chimica Acta* **2005**, *88*, 604-617.
- (12) Chang, C. A.; Chen, Y.-H.; Chen, H.-Y.; Shieh, F.-K. *Journal Of The Chemical Society-Dalton Transactions* **1998**, 3243-3248.
- (13) Pasha, A.; Tircsó, G.; Benyó, E. T.; Brücher, E.; Sherry, A. D. *European Journal Of Inorganic Chemistry* **2007**, *27*, 4340-4349.
- (14) Baranyai, Z.; Bányai, I.; Brücher, E.; Király, R.; Terreno, E. *European Journal Of Inorganic Chemistry* **2007**, *2007*, 3639-3645.
- (15) Chen, R. F. *Analytical Letters* **1967**, *1*, 35 - 42.
- (16) Breen, P. J.; Horrocks Jr., W. D. *Inorganic Chemistry* **1983**, *22*, 536-540.
- (17) Kimura, T.; Kato, Y. *Journal Of Alloys And Compounds* **1998**, *278*, 92-97.
- (18) Gil, V. M. S.; Oliveira, N. C. *Journal of Chemical Education* **1990**, *67*, 473-478.
- (19) Voivodov, K. I.; Ching, J.; Hutchens, T. W. *Tetrahedron Letters* **1996**, *37*, 5669-5672.
- (20) Strother, T.; Hamers, R. J.; Smith, L. M. *Nucleic Acids Research* **2000**, *28*, 3535-3541.
- (21) Wang, H.; Fang, Y.; Cui, Y.; Hu, D.; Gao, G. *Materials Chemistry and Physics* **2002**, *77*, 185-191.
- (22) Nandivada, H.; Jiang, X.; Lahann, J. *Advanced Materials* **2007**, *19*, 2197-2208.
- (23) Parker, D. *Chemical Society Reviews* **1990**, *19*, 271-291.
- (24) Bottrill, M.; Kwok, L.; Long, N. J. *Chemical Society Reviews* **2006**, *35*, 557-571.
- (25) Burchardt, C.; Riss, P. J.; Zoller, F.; Maschauer, S.; Prante, O.; Kuwert, T.; Roesch, F. *Bioorganic & Medicinal Chemistry Letters* **2009**, *19*, 3498-3501.
- (26) Caravan, P. *Chemical Society Reviews* **2006**, *35*, 512-523.

## FIGURES

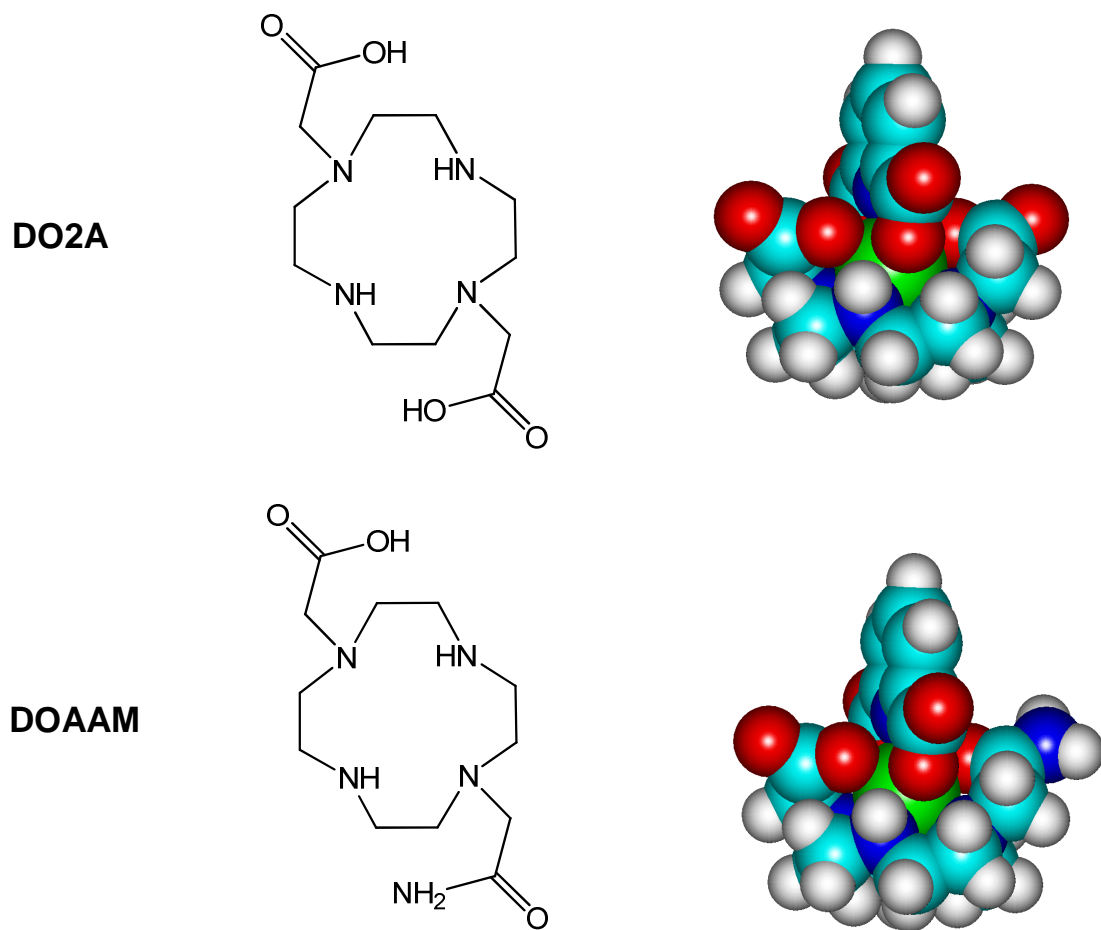


Figure 4.1. Structures of the DO2A and DOAAM macrocyclic ligands, with space-filling models of the Tb(ligand)(dipicolinate) ternary complexes.

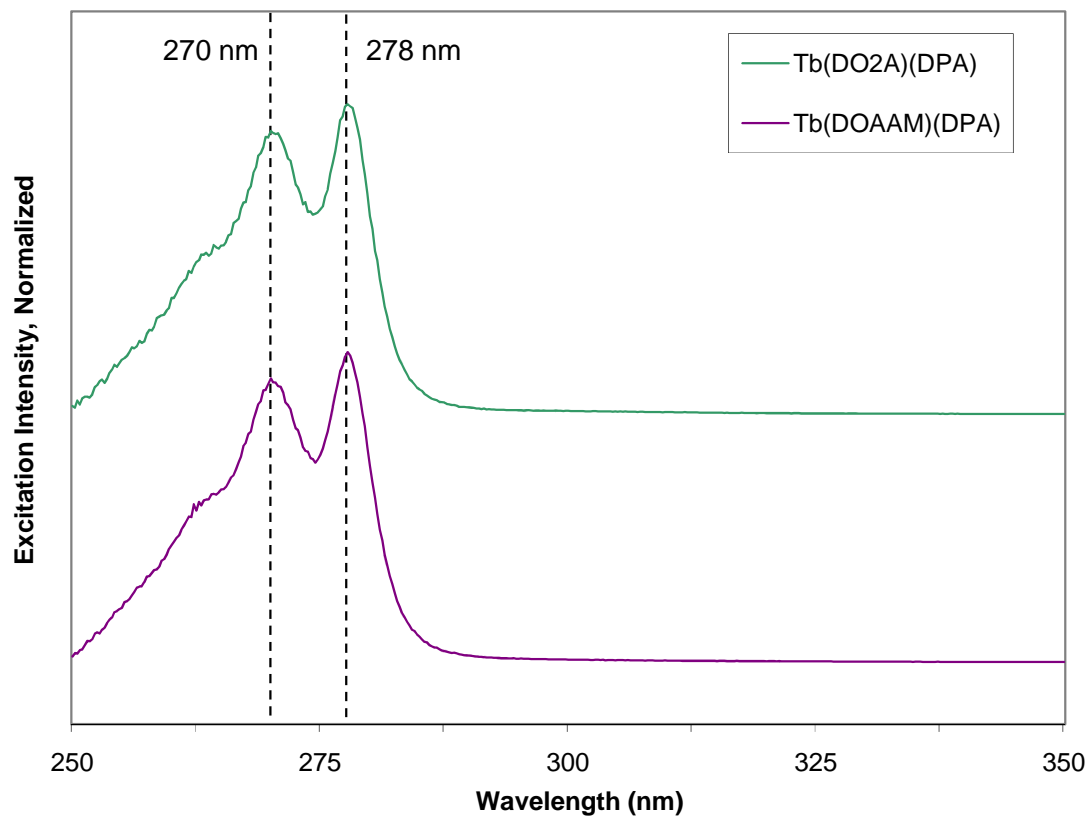


Figure 4.2. Excitation spectra of terbium dipicolinate ternary complexes with DO2A (green) and DOAAM (purple), 10.0  $\mu$ M in 0.1 M MOPS buffer (pH 7.3). The normalized spectra are perfectly superimposable. Relevant transitions are identified with vertical dotted lines (black).

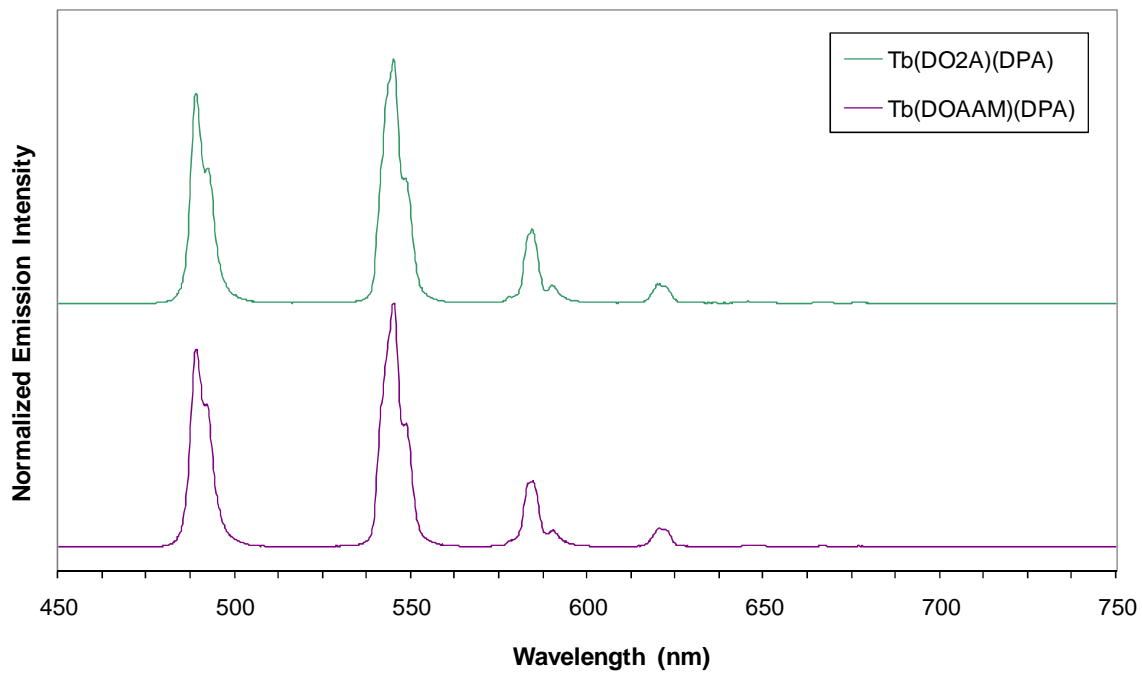


Figure 4.3. Emission spectra of terbium dipicolinate ternary complexes with DO2A (green) and DOAAM (purple), 10.0  $\mu\text{M}$  in 0.1 M MOPS buffer (pH 7.3). The identical splitting indicates that the  $\text{Tb}^{3+}$  is in a similar coordination environment in both complexes.

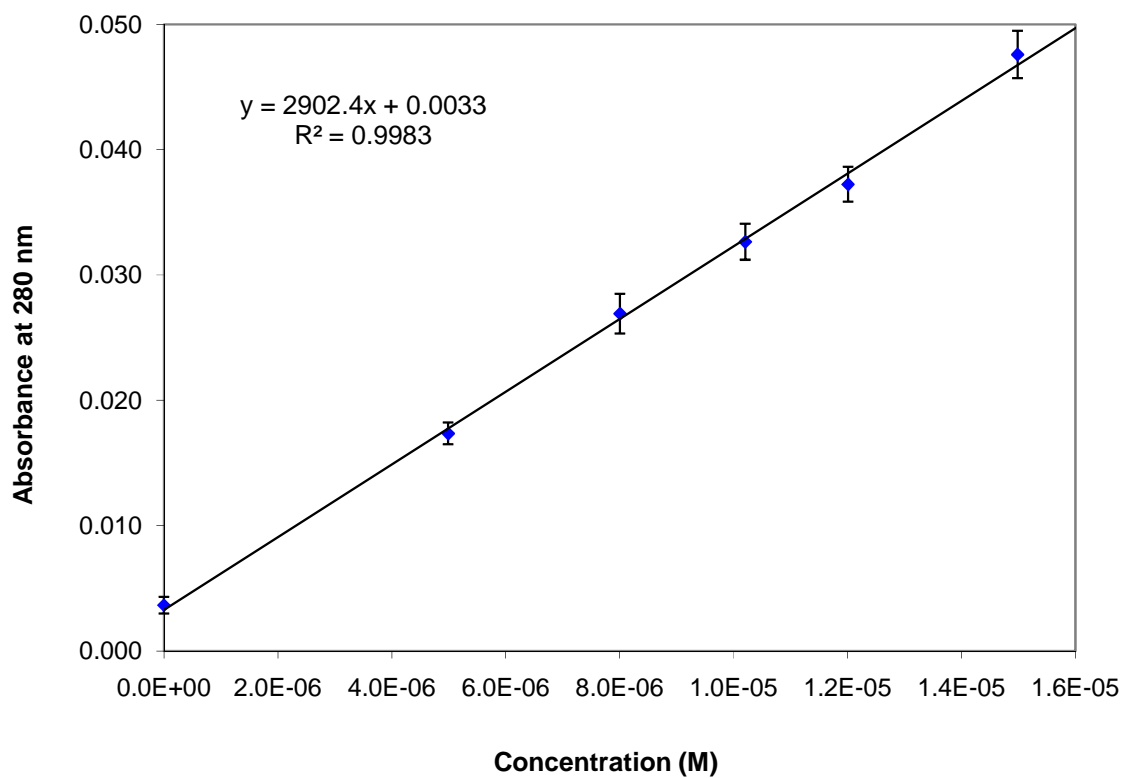


Figure 4.4. Linear fit of absorbance ( $\lambda_{\text{abs}} = 280 \text{ nm}$ ) versus concentration for the Tb(DOAAM)(DPA) complex in 0.1 M Tris buffer, pH 7.9, 25 °C.

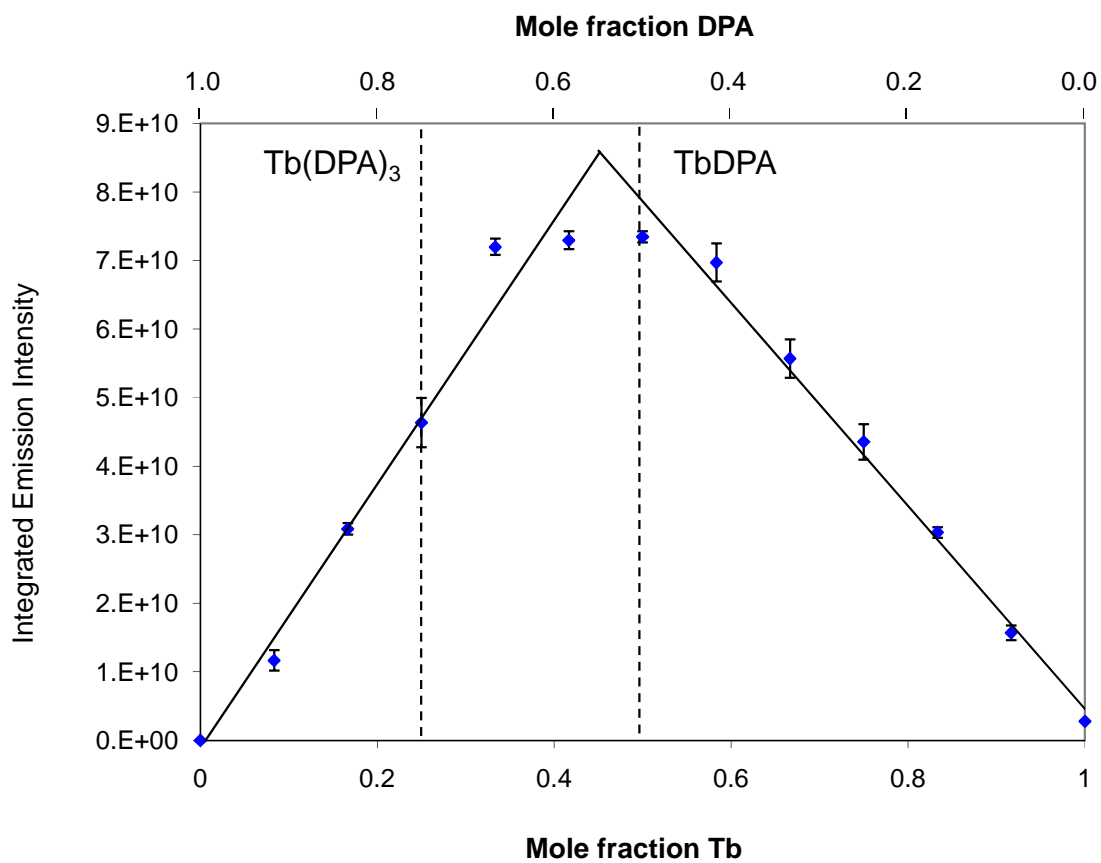


Figure 4.5. Jobs plot of Tb(DOAAM)(DPA) in 0.2 M NaOAc, pH 7.4. The concentrations of Tb and DPA are varied inversely from 0 to 12  $\mu\text{M}$  in 1  $\mu\text{M}$  increments, with the macrocyclic ligand in excess (100  $\mu\text{M}$ ).  $\lambda_{\text{ex}} = 278$  nm, emission integrated from 570–600 nm. Linear regions are fitted with trendlines, and significant Tb:DPA ratios are noted by dashed lines.

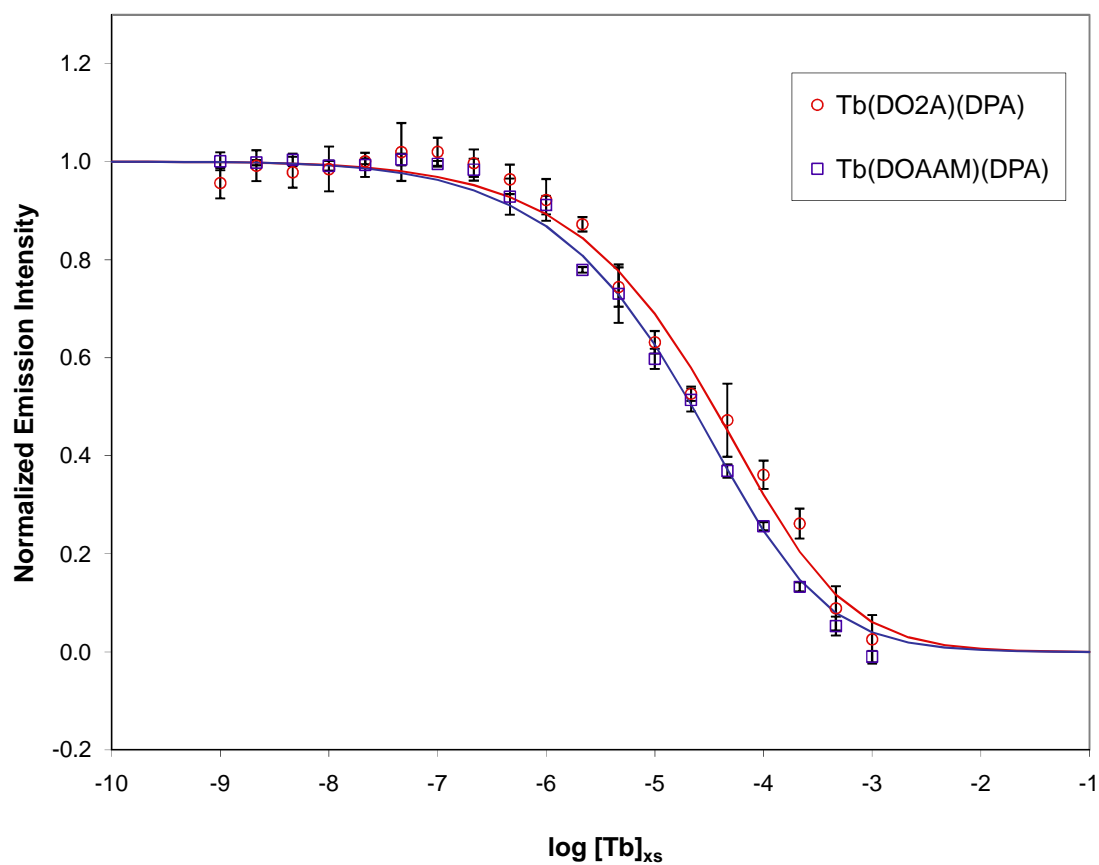


Figure 4.6. Lanthanide competition experiment for  $Tb(DO2A)(DPA)^-$  and  $Tb(DOAAM)(DPA)$ . Binding affinity by competition (BAC) assay titration curves in 0.2 M NaOAc, pH 7.5, 25 °C.  $\lambda_{ex} = 278$  nm, emission intensity integrated over 570–600 nm.

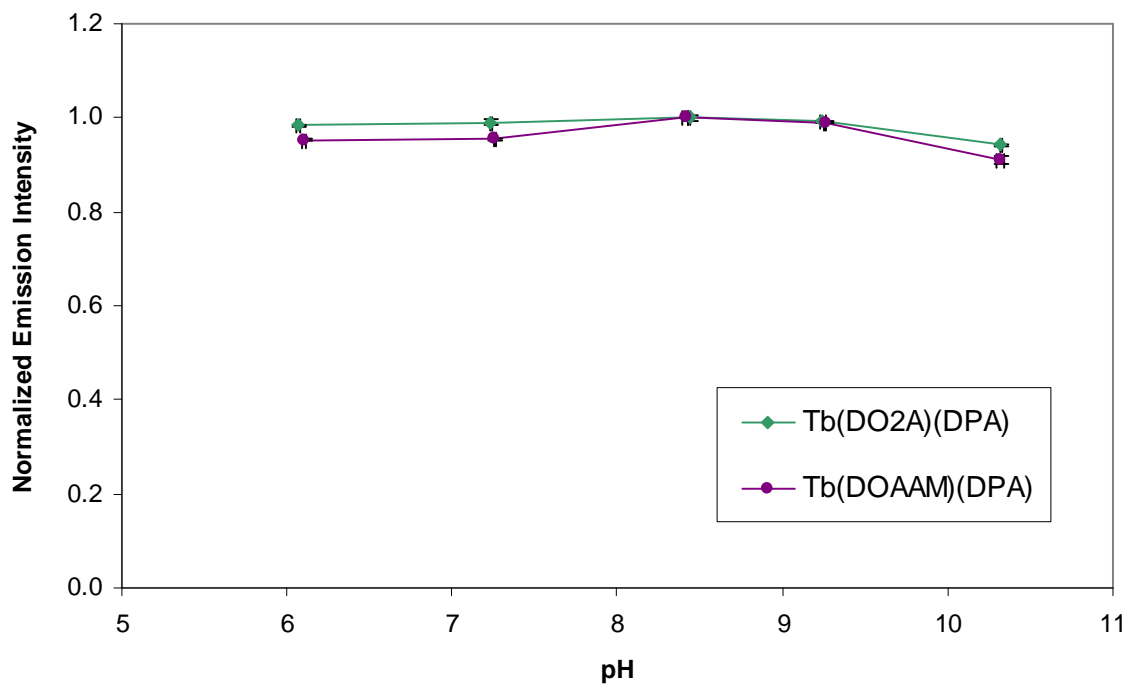


Figure 4.7. pH dependence study of  $\text{Tb}(\text{DO2A})(\text{DPA})^-$  and  $\text{Tb}(\text{DOAAM})(\text{DPA})$  in 0.1 M buffer, 25 °C. Emission integrated from 530–560 nm and normalized to maximum value. ( $\lambda_{\text{ex}} = 278 \text{ nm}$ )

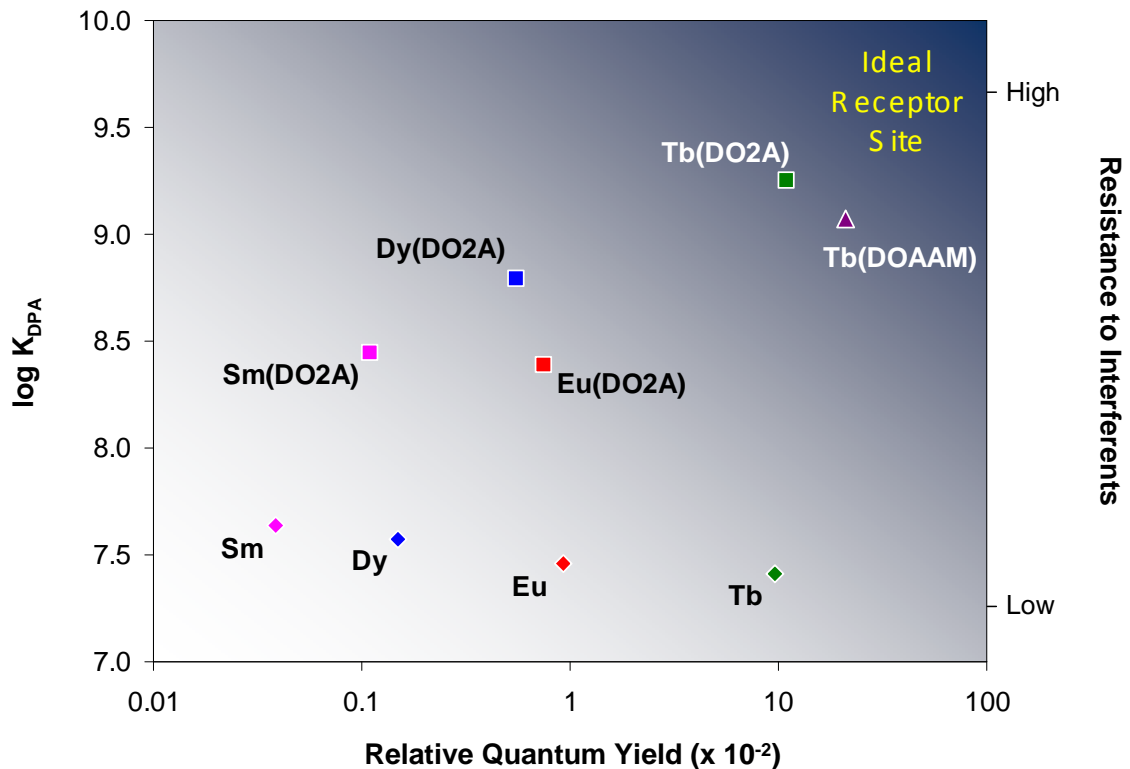


Figure 4.8. Graphic depicting our current improvements of a DPA receptor site in terms of DPA binding affinity ( $\log K_{DPA}$ ), relative quantum yield, and resistance to interferents. The use of Tb along with the DO2A and DOAAM ligands has allowed us to move closer towards development of an ideal receptor site.

## TABLES

Table 4.1. Stability constants of various lanthanide macrocycle complexes.

$\text{Ln}^{3+}$	DOTA <sup>†</sup>	DOTAM <sup>‡</sup>
Eu	23.5	13.8
Gd	24.7	13.1
Dy	24.2	13.6

<sup>†</sup> Reference 12; <sup>‡</sup> Reference 13

Table 4.2. Luminescence quantum yield data, 0.1 M Tris buffer, L-Trp standard.

Complex	Temp (°C)	pH	$\Phi_L$ ( $\times 10^{-3}$ )
Tb(DO2A)(DPA) <sup>-</sup>	24.8 ± 0.2	7.93 ± 0.01	110 ± 2
Tb(DOAAM)(DPA)	24.5 ± 0.3	7.92 ± 0.20	210 ± 7

Table 4.3. Calculated association constants ( $K_a'$ ) for terbium macrocycle complexes with dipicolinate in 0.2 M NaOAc.

Ligand	Temp (°C)	pH	log $K_a'$
DO2A	25.0 ± 0.2	7.36 ± 0.09	9.25 ± 0.13
DOAAM	24.8 ± 0.4	7.52 ± 0.06	9.07 ± 0.02